Synthesis of 5-benzyl-5-((5-nitropyridin-3yl)methyl)-1,3,5-dithiazinan-5-ium through one-pot reactions, characterization and study as a corrosion retardant in high salinity oil fields.

Mushtaq J. Meften, Ammar A. Kadhim

Department of Chemistry, College of Education-Qurna, University of Basrah, Basrah, Iraq.

ARTICLE INFO	ABSTRACT

This study included the preparation of a new heterocyclic compound namely 5-benzyl-5-((5-nitropyridin-3-yl) methyl)-1,3,5-dithiazinan-5-ium (BNPD) by a simple powerful method and an environmentally acceptable. The BNPD compound contains O, N, and S heteroatoms that have been inserted into the chemical structure by one step consisting of several transformations. The BNPD structure has been characterized using several techniques like FT-IR, ^{1}H-NMR, ^{13}C-NMR, and G-C mass. The prepared molecule has been studied as an inhibitor of carbon steel corrosion (N-80), which is generally used in oil fields. The BNPD effectiveness has been studied as an anti-corrosive material in saline water that accompanies the extraction of crude oil. Saline water contains dissolved solids estimated at 239581mg/l, conductivity 254.23 ms/cm, and pH 6.1. The retardant has been evaluated by electrochemical impedance spectroscopy technique (EIS), potentiodynamic polarization technique (PP), scanning electron microscopy-energy dispersive x-ray spectroscopy (SEM/EDX), and weight loss method (WL) at 308K($\pm$1). It was noted that inhibition efficiency increases with increasing BNPD concentration. The results of potentiodynamic polarization showed that the studied inhibitor molecules act as a mixed-type inhibitor, while the results of weight loss showed that these molecules adsorbed on the carbon steel surface through physical and chemical adsorption simultaneously. The results of the SEM/EDX indicated that slight corrosion occurred at the inhibitor was added, where the EDX spectrum of N-80 at 80 mg.dm^{-3} of inhibitor was noticed approximately similar to the polished carbon steel spectrum. Furthermore, the electronic and physic-chemical characteristics of BNPD have been calculated like E_{HOMO}, E_{LUMO}, energy gap, total energy, lipophilicity coefficient, molecule surface area, molecular volume, molecular polarizability, molar refractivity, dipole moment, solvation energy, theoretical inhibition efficiency, and electrostatic potential surfaces. The BNPD compound has shown wonderful results in corrosion inhibiting, where its efficiency optimum reached 91.14%, 93.60%, and 93.46% for WL, EIS, and PP techniques, respectively. Either theoretical efficiency reached 90.25%.

1. Introduction

Corrosion is a well-known phenomenon and a common problem in oil production facilities and its transportation for many years until this day, its economic implications cost millions of dollars every

year [1-2]. The total cost resulting from corrosion processes of all kinds has been estimated from 3% to 5% of the gross national product of industrial countries. The total losses resulting from corrosion damages in oil and gas production facilities and their transportation reached 1.372 billion dollars every year [3]. The risk of corrosion in industries, oilfields, and equipment is caused by the presence of water and hydrocarbons. A few water drops are sufficient to emergence the corrosion thus excessive losses occur [4]. The corrosion of each oil field, gas well, and pipeline manifest itself in various types, among them sweet corrosion (corrosion caused by carbon dioxide), sour corrosion (corrosion caused by hydrogen sulfide), and corrosion caused by dissolved oxygen in the water. These types are considered the most prevalent in oilfields and petroleum industries. Dissolved gases like oxygen, carbon dioxide, and hydrogen sulfide increase the rate of oilfield corrosion. Dissolved oxygen is considered a potent oxidizer agent and plays an essential role in corrosion increase [3,5]. Recently, the corrosion caused by carbon dioxide has been given much attention, because of its injection increase into oil wells to reduce its viscosity and increase its production. Metals inhibition and their alloys are considered very important and it practiced widely in petroleum and chemical industries. The best way to decrease corrosion caused by CO_2 is to use nitrogen-containing organic molecules. The corrosion of steel caused by dissolved CO_2 gas is considered a complicated electrochemical process, which includes the dissolution of the iron on the anode and then the evolutes of hydrogen on the cathode [4,6,7]. Retardants are chemical substances that have a significant influence on reducing corrosion, and they are usually added in small concentrations to the corrosive environment to minimize or prevent corrosion [8]. The use of inhibitors is considered one of the best methods which effectively secures oil pipelines against corrosion [9-11]. The organic compounds that possess (i) polar functional groups like – CHO, − NH_2, −NO_2,−CN,−SH,−OH, and so on, (ii) π- electrons (iii) aromatic rings having multiple bonds, (iv) hetero atoms like nitrogen, oxygen, sulfur, and phosphor whether inside the ring or in its side chain. They are considered active inhibitors against corrosion because contain the centers which facilitate the adsorption processes on metal surfaces hence decreasing their dissolution [12-15]. The mechanisms of corrosion inhibition are often different, and impossible to assign a single predominant mechanism for all inhibitors due to experimental properties differences like concentration of retardant, the density of metal, corrosive environment, nature of the metal, temperature, and inhibitor structure, etc. [16]. Domino reactions (one-pot reactions) are eco-friendly cascade reactions and are considered one of the best powerful ways in organic synthesis due to the formation of several bonds in one step through several transformations under the same conditions. Domino reactions are used to prepare the complicated heterocyclic molecules from simple chemicals in one pot, like the preparation of 6-methyl-3-thia-1,5-diazabicyclo [3.2.2] nonane. In general, modern domino reactions include the preparation of heterocyclic compounds containing oxygen, nitrogen, and sulfur atoms together without isolating the intermediate compounds that formed in the previous step, like the preparation of 2-oxa-4,8,10-trithia-6,12,15-triazatricyclo [9.3.1] pentadeca-1(15),11,13-triene [17-21]. The main aim of the current study is to reduce the economic cost resulting from oil field corrosion and their facilities in oil producer countries. Therefore, the compound 5-benzyl-5-((5-nitropyridin-3-yl) methyl)-1,3,5-dithiazinan-5-ium (BNPD) was prepared as a novel inhibitor against oilfields corrosion. The results of BNPD molecules indicated an excellent role in inhibition.

2. Experimental details.

2.1. Materials specifications.

In general, the main metal used in the oilfields and their equipment is carbon steel No. N-80 is versatile, such as it's used in flow lines of petroleum, transmission pipelines, and construction material

for downhole tubular. From Basra oil company IRAQ, it was supplied. Carbon steel sample was analyzed in MET-CHEM Laboratories, Baroda, India, its chemical composition is a C (0.31%), Mn (0.92%), Cr (0.20%), P (0.01%), S(0.008%), Si(0.19%) and Fe(98.362%) [22]. For corrosion experiments studied by the weight loss method and SEM/EDX technique, the carbon steel sheet was cut into coupons in dimensions 0.5cm, 3cm, and 7cm for thickness, width, and length respectively, therefore the area of every coupon became $52cm^2$. To study corrosion inhibition by the potentiodynamic and impedance techniques, the N-80 sheet was cut into coupons in dimensions 1cm and 0.5cm for diameter and thickness respectively. The coupons were polished mechanically and then manually carefully with SiC papers (300, 600, 800, and 1200 grit size), then were cleaned of distilled water, absolute ethanol, and acetone respectively. Finally, were kept in a moisture-free desiccator for about 5 hours, then under an N_2 atmosphere were stored to be used in corrosion experiments. The corrosive environment is saline water accompaniment for crude oil extract and its supplier from west Qurna wells high salinity. The physicochemical characteristics of saline water were determined, where the conductivity 254.23 ms/cm, pH 6.1, total suspended solids 74.22 mg/l, and total dissolved solids 239581mg/l were measured. Also, the concentration of each of the chloride, sulfate, calcium, magnesium, potassium, and sodium in mg/l was determined where reached 164599, 1987, 17650, 5349, 1270, and 48733, respectively. All chemicals used in this study were procured from Merck and Sigma-Aldrich. The schematic structure of 5-benzyl-5-((5-nitropyridin-3-yl) methyl)-1,3,5-dithiazinan-5-ium was shown in Fig1.
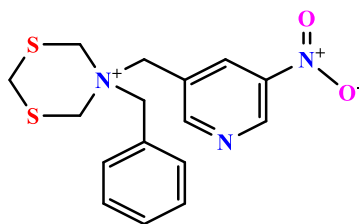

Fig.1. Schematic structure of BNPD

2.2. Properties and data of devices

FT-IR spectrum of BNPD compound was recorded at KBr disc in a range 400–4000 cm^{-1} using a device it's model SHIMADZU-620. ^{1}H-NMR and ^{13}C NMR spectra were recorded at a Bruker device it's model BM400MHz by DMSO-*d*6 as a solvent. G-C mass spectra have been recorded in the SHIMADZU device it's model GCMS-Q2014. Where 0.5 ml of the sample was injected at a flow rate of 0.3 ml/min. Oven temperature has been programmed beginning with 40°C for 1min increased to 300°C by rate 10ºC/min. Helium gas was used as a carrier medium with a purity of 99.995%, the injector temperature was set at 300ºC. Furthermore, the mass spectra were recorded at ionization voltages of 70eV and 250ºC. Polarization curves of prepared inhibitor have been recorded using a device its model CHI660B/400S. The scan rate of open circuit potential (OCP) is 0.1 mVs^{-1} and has been established within 6 min. Typical Tafel curves were recorded at polarization potential scanning from -600 mV to 200 mV. Impedance curves have been recorded by using the software of a device its model CHI660D at a frequency range from 1000Hz to100 mHz in OCP with an amplitude of 10 mV/s peak to peak. The electrochemical experiments of PP and EIS techniques were carried out in a double glass cell its size of 300ml. The corrosion cell consists of three electrodes, platinum as the auxiliary electrode, standard calomel electrode SCE as the reference electrode, and carbon steel N-80 as the working electrode. Microscopic images of SEM and spectra of EDX have been recorded using a device its model JSM–6600LW under a voltage of 15 kV. Carbon steel specimens were gently rinsed with deionized water and under the nitrogen gas were dried before conducting a test of SEM.

2. 3. Corrosion calculations

In weight loss experiments, the corrosion rate (C_R) has been calculated in (mg cm^{-2}h^{-1}) through equation 1, where W is the weight loss represented in N-80 in mg unit, A is the total area of the N-80 surface (52cm^2), T is the exposure time of carbon steel in saline water in hr. unit [23,24]. Inhibition efficiency (E_I) has been calculated using equation 2, where $C_R{}^{inh}$ and $C_R{}^o$ are the corrosion rate with and without inhibitor, respectively [25]. Equation 3 was used to surface coverage (θ) calculate [26].

$$C_R = \frac{W}{T\,A} \qquad\qquad (1)$$

$$E_I(\%) = \frac{C_R{}^o - C_R{}^{inh}}{C_R{}^o} \times 100\% \qquad (2)$$

$$\theta = \frac{C_R{}^o - C_R{}^{inh}}{C_R{}^o} \qquad\qquad (3)$$

In EIS experiments, the inhibition efficiency, surface coverage, and double layer capacitance (C_{dl}) of Randle's circuit have been calculated using equations 4, 5 and 6, respectively [27], where $R_{ct(free)}$ and $R_{ct\,(inh)}$ are a charge transfer resistance in the absence and presence of inhibitor, respectively, while the f_{max} is maximum frequency. Equation 7 was used for the excess positive potential on the surface (E_P) calculate [28], where E_{ocp} and E_{pzc} are the open circuit potential and the potential of zero charges, respectively. The time constant of the charge transfer process (τ_d) has been calculated using equation 8 [29]. The charge transfer resistance (R_{ct}) has been calculated by intersecting the fitted semicircle with the real axis (Z_{real}) at the low frequency, while the solution resistance R_s was calculated by intersecting the fitted semicircle with the real axis (Z_{real}) at the high frequency. The R'_{ct} includes the charge transfer resistance and diffusion layer resistance at the working electrode and was calculated as described in equation 9 [7].

$$E_I(\%) = \left(1 - \frac{R_{ct\,(free)}}{R_{ct\,(inh.)}}\right) \times 100\ \% \qquad (4)$$

$$\theta = \left(1 - \frac{R_{ct\,(free)}}{R_{ct\,(inh.)}}\right) \qquad\qquad (5)$$

$$C_{dl} = \frac{1}{2\pi\,f_{max}\,R_{ct}} \qquad\qquad (6)$$

$$E_p = E_{ocp} - E_{pzc} \qquad\qquad (7)$$

$$\tau_d = C_{dl} \times R_{ct} \qquad\qquad (8)$$

$$R'_{ct} = R_{ct} - R_s \qquad\qquad (9)$$

In polarization experiments, the inhibition efficiency and surface coverage have been calculated using equations 10 and 11 respectively [30], where I_{corr}^o and I_{corr}^{inh} are corrosion current density in the absence and presence of an inhibitor, respectively. Potential displacement ΔE_{corr} has been calculated using equation 12 [31], where E_{corr}^o and E_{corr}^{inh} are the corrosion potential in the absence and presence of inhibitor, respectively. Also, the inhibition efficiency $\eta\%_{R_p}$ was calculated from linear polarization using equation 13 [32], where R_{pi} and R_{po} are polarization resistance with and without inhibitor, respectively.

$$E_I(\%) = \frac{I_{corr}^o - I_{corr}^{inh}}{I_{corr}^o} \times 100\ \% \qquad (10)$$

$$\theta = \frac{I_{corr}^o - I_{corr}^{inh}}{I_{corr}^o} \qquad (11)$$

$$\Delta E_{corr} = E_{corr}^{inh} - E_{corr}^o \qquad (12)$$

$$\eta\%_{R_p} = \frac{R_{pi} - R_{po}}{R_{pi}} \times 100\% \qquad (13)$$

In SEM/EDX experiments the percentage of corroded iron (% Fe loss) was calculated as described in equation 14 ,where % E^o and % E are the percentage of iron in fresh carbon steel and the percentage of iron in carbon steel after corrosion, respectively. The inhibition efficiency (IE %) was calculated by using the equation15, where, % Fe loss and % Fe^oloss are the percentage of corroded iron with and without inhibitor, respectively [17].

$$\% \text{ Fe loss } = \frac{\%E^o - \%E}{\%E^o} \times 100 \qquad (14)$$

$$\% \text{ IE} = \frac{\%Fe^o \text{ loss} - \%Fe \text{ loss}}{\%Fe^o \text{ loss}} \times 100 \qquad (15)$$

3. Results and discussion

3. 1. Synthesis and characterization of BNPD compound

The compound 5-benzyl-5-((5-nitropyridin-3-yl) methyl)-1,3,5-dithiazinan-5-ium (BNPD) was prepared by domino reactions, where the reaction pot consists of (5-nitropyridin-3-yl)methenamine, 36% formaldehyde, and hydrogen sulfide gas in 1:3:3 ratios respectively, then the benzyl chloride was added to it. The mixture of reaction (3.06g; 20mmol) of (5-nitropyridin-3-yl)methenamine, (5ml; 60mmol) of the aqueous solution of formaldehyde and 80ml ethanol have been put in one pot with stirred for about 1hr at 0 ℃. Then 60mmol of H_2S gas was added to the mixture in bubble form for 2 hrs., (H_2S gas was prepared by adding the 25ml of HCl in the form of drops to14.4 g of sodium sulfide nonahydrate $Na_2S.9H_2O$). The organic layer was separated by chloroform and was dried by sodium sulfate then under nitrogen gas was evaporated to produce a light yellow compound of 5-((5-nitropyridin-3-yl) methyl)-1,3,5-dithiazinane (NPMD). Finally, (1.4ml; 10mmol) of benzyl chloride and 60ml of absolute ethanol have been added to (2.57g; 10mmol) of NPMD compound with stirred for 8 hrs at 40℃ to produce a white compound of 5-benzyl-5-((5-nitropyridin-3-yl) methyl)-1,3,5-dithiazinan -5-ium(BNPD). Color: White powder; Yield: 48%; m.p. 234-236℃. FT-IR (KBr,ν_{max}/cm^{-1}): $\nu_{CH- aromatic}$ =3160.93cm^{-1}; $\nu_{CH- aliphatic}$=2983.88cm^{-1}; ν_{C-N}=1240.23cm^{-1}; $\nu_{C=C}$=1600.92cm^{-1}; $\nu_{C-S (br)}$= 640.00cm^{-1}; $\nu_{N=O symmetric}$= 1399.46 cm^{-1}; $\nu_{N=O asymmetric}$=1490.91cm^{-1}; $\nu_{C=N}$=1708.93 cm^{-1} as shown in Fig. 2. ^{1}H-NMR (400 MHz, DMSO-d_6, δ, ppm): 2.52 (s, DMSO-d_6); 3.7-4.7 (br, 4H, S-CH$_2$-N); 5.22 (s, 4H, N$^+$-CH$_2$-C) ;3.21 (s, 2H, S-CH$_2$-S); 7.2-7.4 (m, 5H, aromatic benzene ring); 8.3-8.5 (m, 3H, pyridine ring) as shown in Fig.3. ^{13}C-NMR (400 MHz, DMSO-d_6, δ, ppm): 35.09 (C$_1$,S-C-S); 59.22 (2C$_2$, N$^+$ -CH$_2$-C); 63.00 (2C$_3$,S-CH$_2$- N$^+$); carbon signals of aromatic benzene ring are an 125.15(2C$_4$);125.75 (2C$_5$) ;120.03 (C$_6$) ;129.05 (C$_7$);134.05(C$_8$,N-CH-C); 137.22(C$_9$, C-CH-C); 140.07 (C$_{10}$,C-NO$_2$); 142.43 (C$_{11}$, N-CH-C); 143.53 (C$_{12}$,N=CH-C); multiple signals at 38.69 -40.36 for DMSO-d_6 as shown in Fig.5. The G-C spectrum of NPMD proved the synthesis mechanism through the rate time of peaks for formed intermediate compounds as shown in Fig.11. Where the rate time of the C$_8$H$_9$N$_3$O$_3$ peak at 13.8 min was noted and its molecular ion at 195 m/z as evident in Fig.7, while the rate time of the C$_9$H$_{11}$N$_3$O$_4$ peak at 18.3 min was noted and its molecular ion at 225 m/z as evident in Fig.8. Furthermore, the rate time of the C$_9$H$_{11}$N$_3$O$_3$S peak and C$_9$H$_{11}$N$_3$O$_2$S$_2$ peak at 21.0 min and 25.1 min was noted, respectively as shown in Fig.11, while their molecular ions it was noted at 241m/z and 257 m/z as evident in Figs.4 and 9, respectively. From the G-C spectrum of BNPD, it was observed

144

that the rate time of its peak at 15.0 min as shown in Fig.12 and its molecular ion at 348 m/z as evident in Fig.6. MS, m/z (I_{rel},%) of BNPD, the molecular ion at $348[M]^+(29.96)$; $77[C_6H_5]^+(14.07)$; $78[C_5H_4N]^+(36.07)$; $92[C_6H_6N]^+(25.14)$; $91[C_7H_7]^+$ (52.02); $120[C_3H_6S_2N]^+$ (44.07); $134[C_4H_8S_2N]^+(24.81)$; $211[C_{10}H_{13}S_2N]^+(50.02)$; base peak at $123[C_5H_3N_2O_2]^+(100)$; $225[C_{11}H_{15}S_2N]^+$ (12.11); $148[C_5H_{10}S_2N]^+$ (2.02); $271[C_{10}H_{13}N_3S_2O_2]^+(52.81)$; $137[C_6H_5N_2O_2]^+$ (16.02); $257[C_9H_{11}N_3S_2O_2]^+(35.11)$; $302[C_{16}H_{18}N_2S_2]^+(14.14)$; $166[C_3H_6N_2S_2O_2]^+$ (35.45) as shown in Fig.6. The structures of the most important fragments in the mass spectrum of BNPD were showed in Fig.10. Scheme 1 illustrates the synthesis mechanism of the BNPD [33-35].
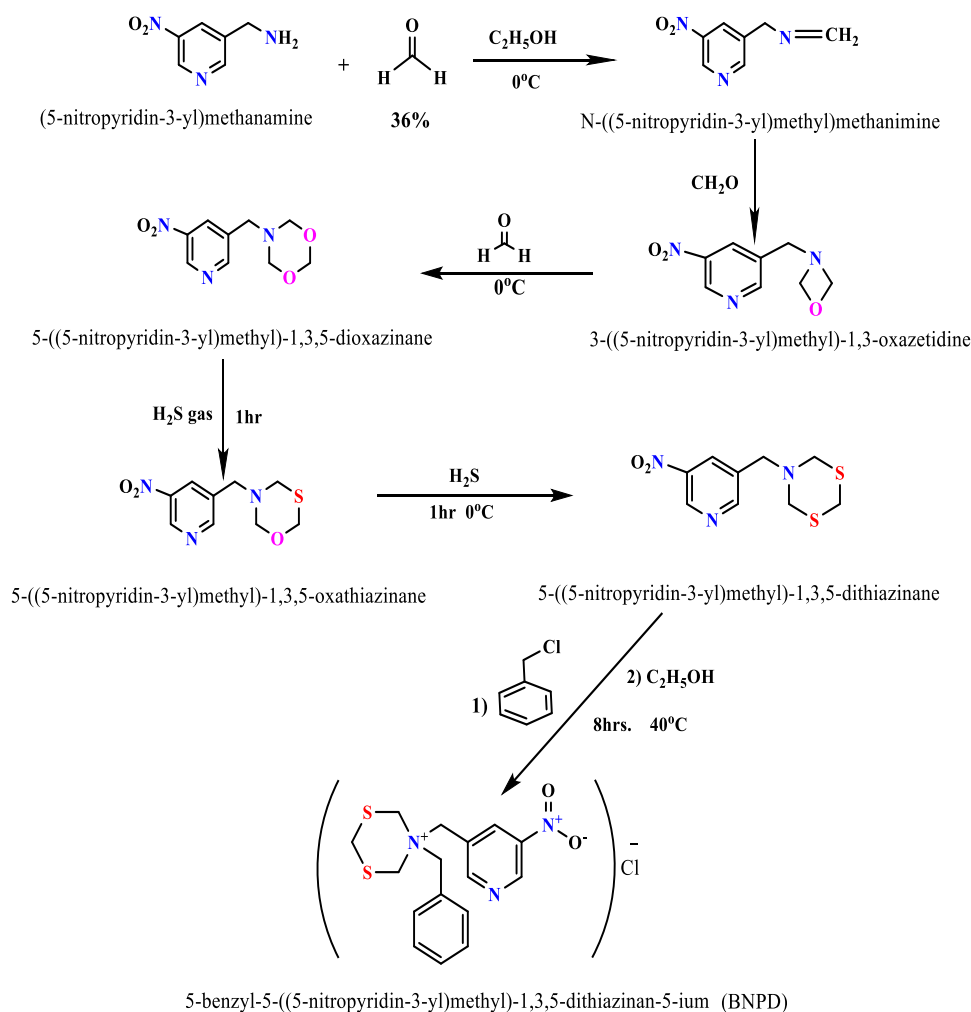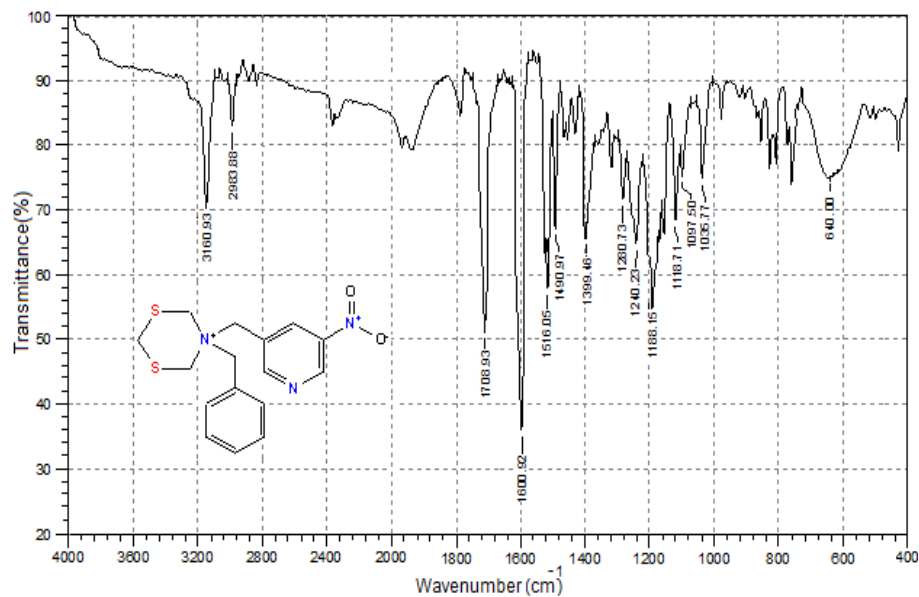

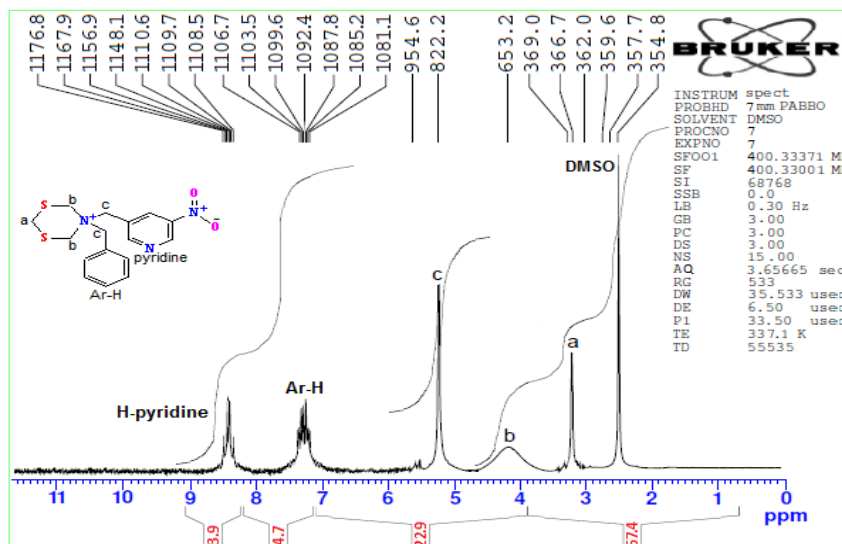**Scheme 1.** Synthesis mechanism of BNPD

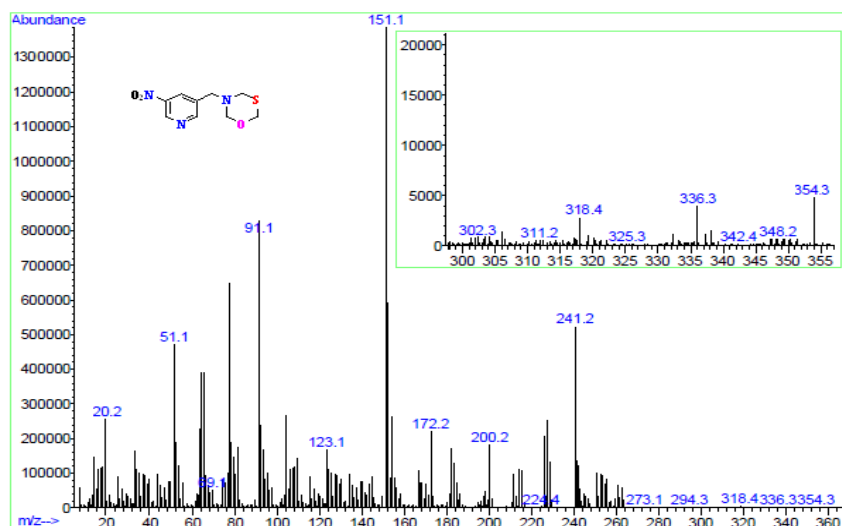**Fig.2.** FT- IR spectrum of BNPD

Fig.3. 1H-NMR spectrum of BNPD.

Fig.4. Mass spectrum of the 5-((5-nitropyridin-3-yl) methyl)-1,3,5-oxathiazinane
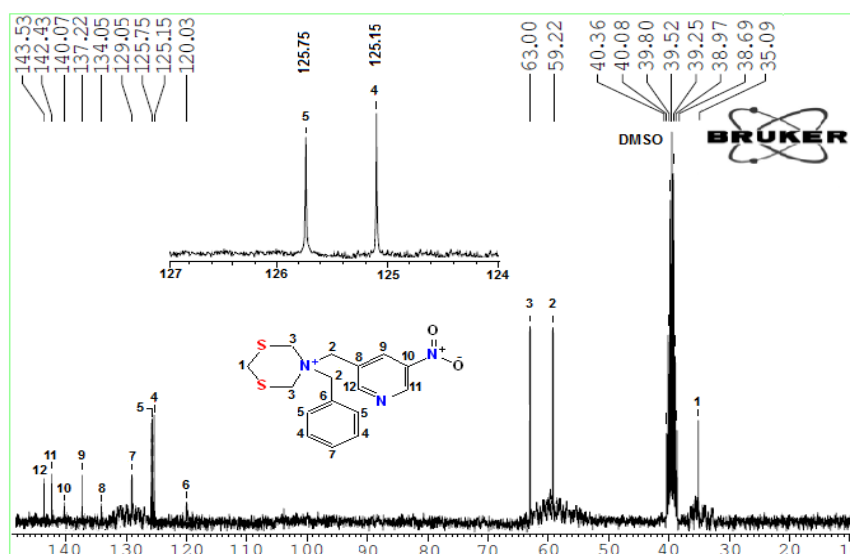
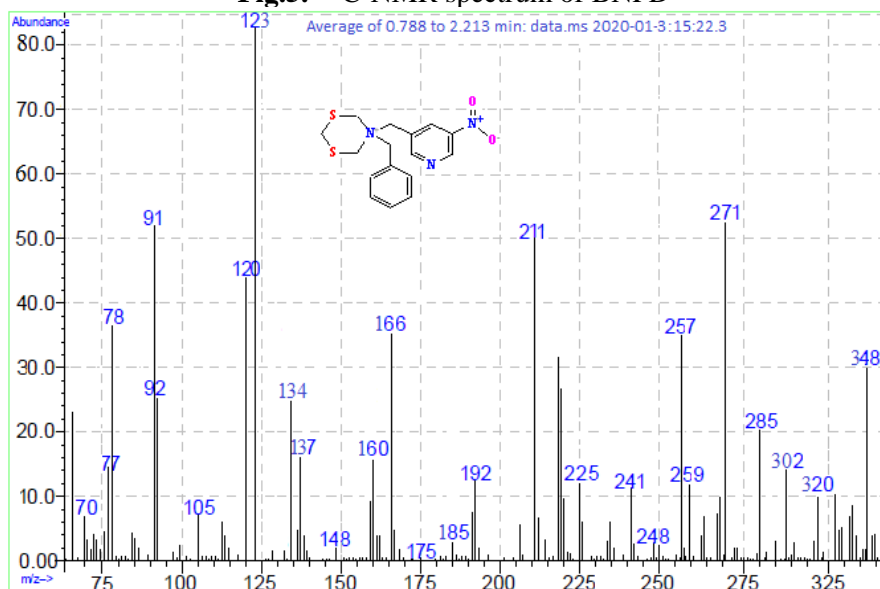**Fig.5.** ^{13}C-NMR spectrum of BNPD

Fig.6. Mass spectrum of BNPD

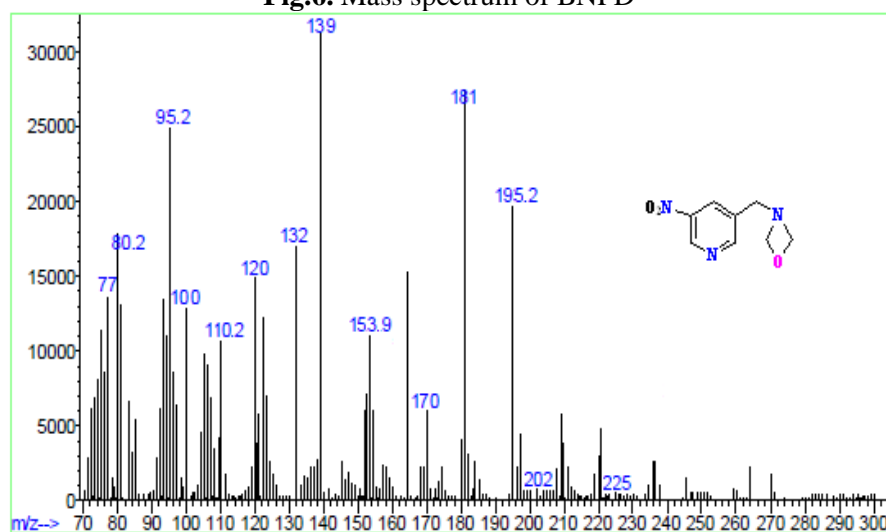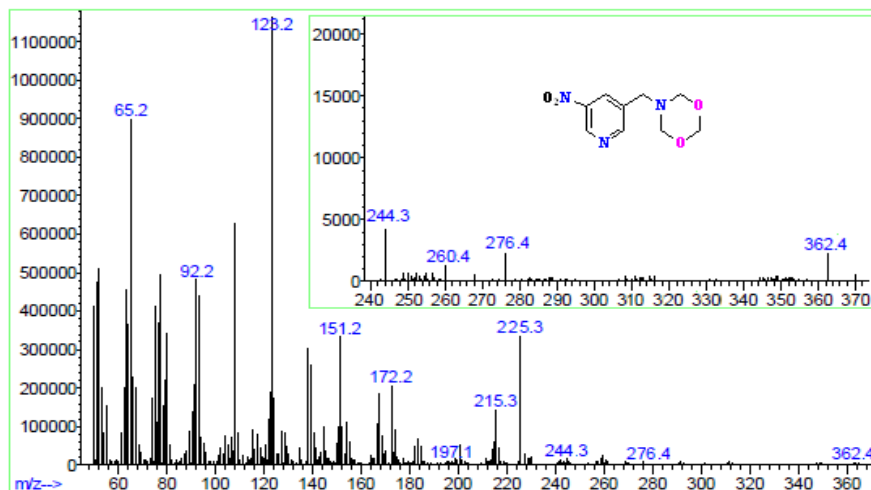**Fig.7**: Mass spectrum of the 3-((5-nitropyridin-3-yl) methyl)-1,3-oxazetidine.

Fig.8. Mass spectrum of the 5-((5-nitropyridin-3-yl) methyl)-1,3,5-dioxazinane

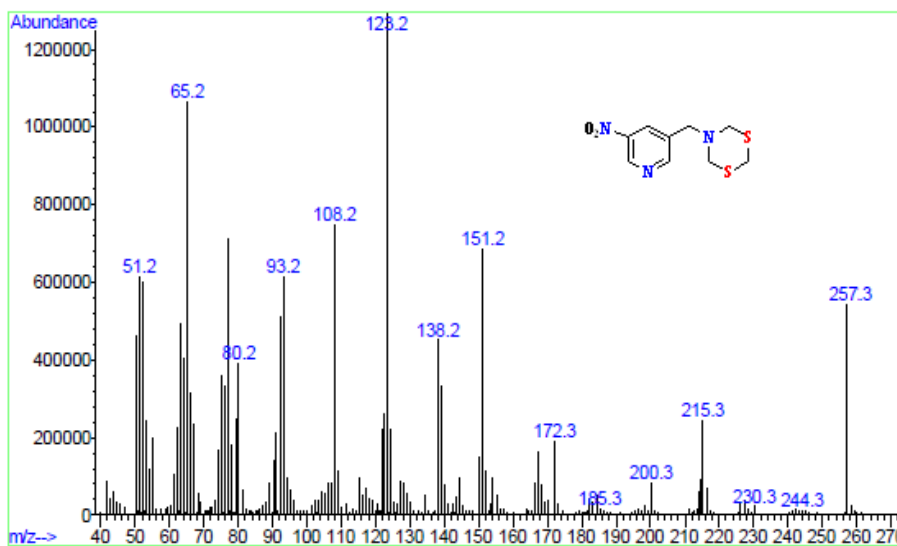
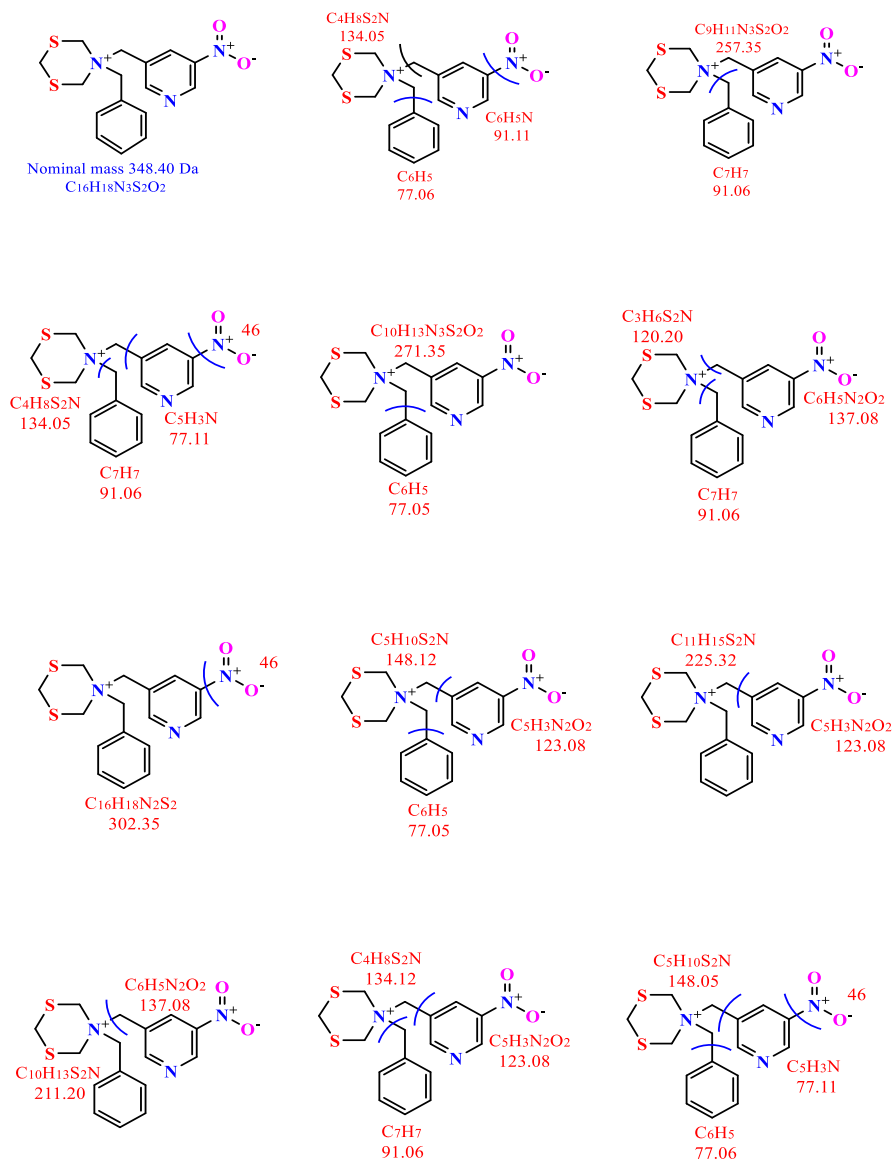**Fig.9.** Mass spectrum of the 5-((5-nitropyridin-3-yl) methyl)-1,3,5-dithiazinane (NPMD)

148

Fig.10. Structures of most important fragments in the mass spectrum of BNPD
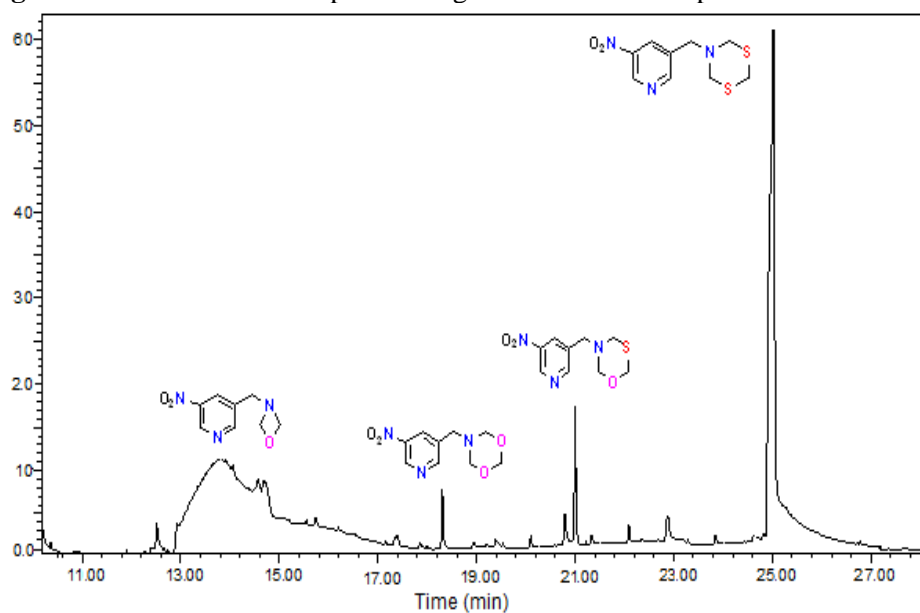

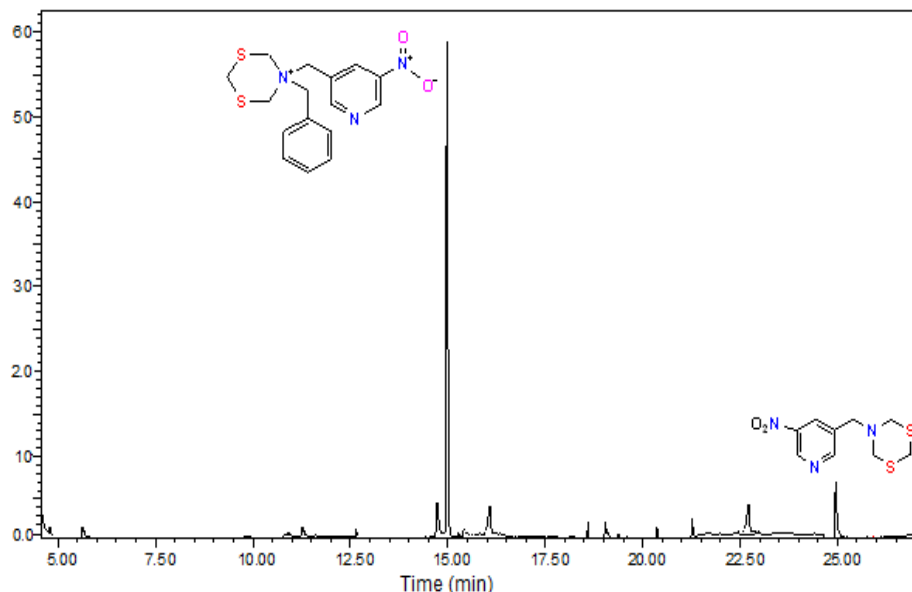**Fig.11.** G-C spectrum of the product of one-pot reaction (NPMD)

Fig.12. G-C spectrum of BNPD

3. 2. Results of inhibition by electrochemical impedance technique

The experiments of EIS were performed under potentiostatic conditions after immersion of the samples in the saline water for 3 hrs. regarding the absence and presence of different concentrations of BNPD. Nyquist diagrams were shown in Fig.13(a), where the concentration increase of BNPD molecules led to the regular gradual increase in the semicircle diameter of the Nyquist curve, which refers to the decrease of corrosion rate. It can be realized that the semicircle of every concentration is regular due to non-dispersion of frequency and this is caused by the homogeneity of the N-80 surface and BNPD adsorption on it easily. That is to say, a slight change has occurred in the inhibition mechanism while the mechanism of corrosion does not change [36-38]. The radius of the capacitive arc in the inhibitor presence is larger than its absence significantly and it increases with increasing inhibitor concentration, this indicates that the efficiency of BNPD molecules increases with its increased concentration [39]. According to inhibitor presence, the charge transfer resistance (R_{ct}) increase is due to the excellent performance of BNPD in adsorption on the N-80 surface, where its effect was wonderful on the resistance of carbon steel corrosion [37]. As Bode-phase angle plots are shown in Fig.13(b), it was noted that a maximum phase angle was shifted towards lower frequency interims of adding inhibitor molecules. This indicates to increase in the constant of the system period [40]. Phase-angle diagrams show that there are two-time constant of the carbon steel in the inhibitor presence. They also reveal two regions of frequency within the system period. The time constant at low-frequency regions can be ascribed forming the double layer, where the charge transfer resistance and capacitive reactance modulus have been increasing significantly. The time constant at the high-frequency region can be ascribed to the forming of the oxide film. Furthermore, the impedance slope in the intermediate frequency region is close to 1 [37,41,42]. In some inhibitor concentrations, one peak and one constant have appeared in the phase angle diagram, pointing to the inhibition properties and coatings being good [37,43]. Bode plots possess similar shapes at all concentrations, which indicates that the mechanism of corrosion is unaffected by adding BNPD molecules [29]. AC impedance increases with increasing inhibitor concentration as evident in Fig.13(c) and this led to an increase in inhibition efficiency [44]. The potential of zero charge (PZC) is the most important method to provide fundamental information about the nature of metallic surfaces and their systems whether the surface charge was positive or negative, also it explains the adsorption phenomenon on surfaces. Furthermore, PZC describes the system of the surface when an electric charge density is zero. In this case, neither cations nor anions

can adsorb through their centers ionic on the surface. The charge of the carbon steel surface was determined by the position of open circuit potential (OCP) according to the PZC position. EIS measurements were applied to different potentials in the sense that C_{dl} plots versus applied electrode potential were obtained as shown in Fig.13(d). The minimum value of C_{dl} has been determined in the saline water containing 80 mg.dm^{-3} of BNPD at 155.11 mV which can be known as the potential of zero charge (PZC) while the E_{ocp} value was determined under the same conditions at 273.78 mV as shown in Fig.13(d1) and Table1. The E_{ocp} value was observed more positive than PZC value, so the excess potential(E_P) on the surface of carbon steel is a positive +118.67 mV (the charge of the N-80 surface is positive) because of the anode dissolution of the N-80. So negative ions adsorb firstly on the surface. Also, the value of each PZC, E_{ocp} and E_P was calculated in the inhibitor's absence and it is less than its presence as shown in Fig.13(d2) and Table 1 [28,45]. Corrosion results of carbon steel in the uninhibited system and inhibited by BNPD molecules were listed in Table 1 as follows, maximum frequency (f_{max}), double layer capacitance (C_{dl}), charge transfer resistance (R_{ct}), solution resistance (R_s), charge transfer with diffusion layer resistance (R'_{ct}), inhibition efficiency(E_I), surface coverage (θ), the time constant of the charge transfer process (τ_d), corrosion rate(C_R), open circuit potential (E_{ocp}), potential of zero charge (PZC) and excess positive potential (E_P). The value of R_{ct} has increased while the value of C_{dl} has decreased with the concentration increase of BNPD. The increase of R_{ct} values ascribes to the formation of a protective film of BNPD molecules on the N-80 surface since the maximum value of R_{ct} reached 307.62 $\Omega \cdot cm^2$ at using 80 mg.dm^{-3} of the inhibitor (optimum inhibition). The (C_{dl}) values decrease due to either decreasing in the local dielectric constant or increase in the double layer thickness or both. This indicates that BNPD molecules inhibited the corrosion of N-80 through their adsorption on the interface of carbon steel [39,46]. Also, the C_{dl} decrease may interpret that the double layer between the charge of the carbon steel surface and the solution will act as an electrical capacitor [47]. The decreasing each of C_{dl} and f_{max} with the regular increase in the τ_d and R_{ct} explain that BNPD molecules were adsorbed regularly on the N-80 surface. The corrosion rate proportionates inversely with charge transfer resistance [48] that the R_{ct} increase led (from 34.76 Ωcm^2 to 307.62 Ωcm^2) to the decrease of the corrosion rate from (1.129mpy to 0.193mpy). The inhibition efficiency has increased significantly with increasing of BNPD concentration, it reached 93.6 % which is considered optimal efficiency for inhibition. Also, it can be noted that the result of R_s does not change significantly with inhibitor concentration increase such a change is not at the same pace.
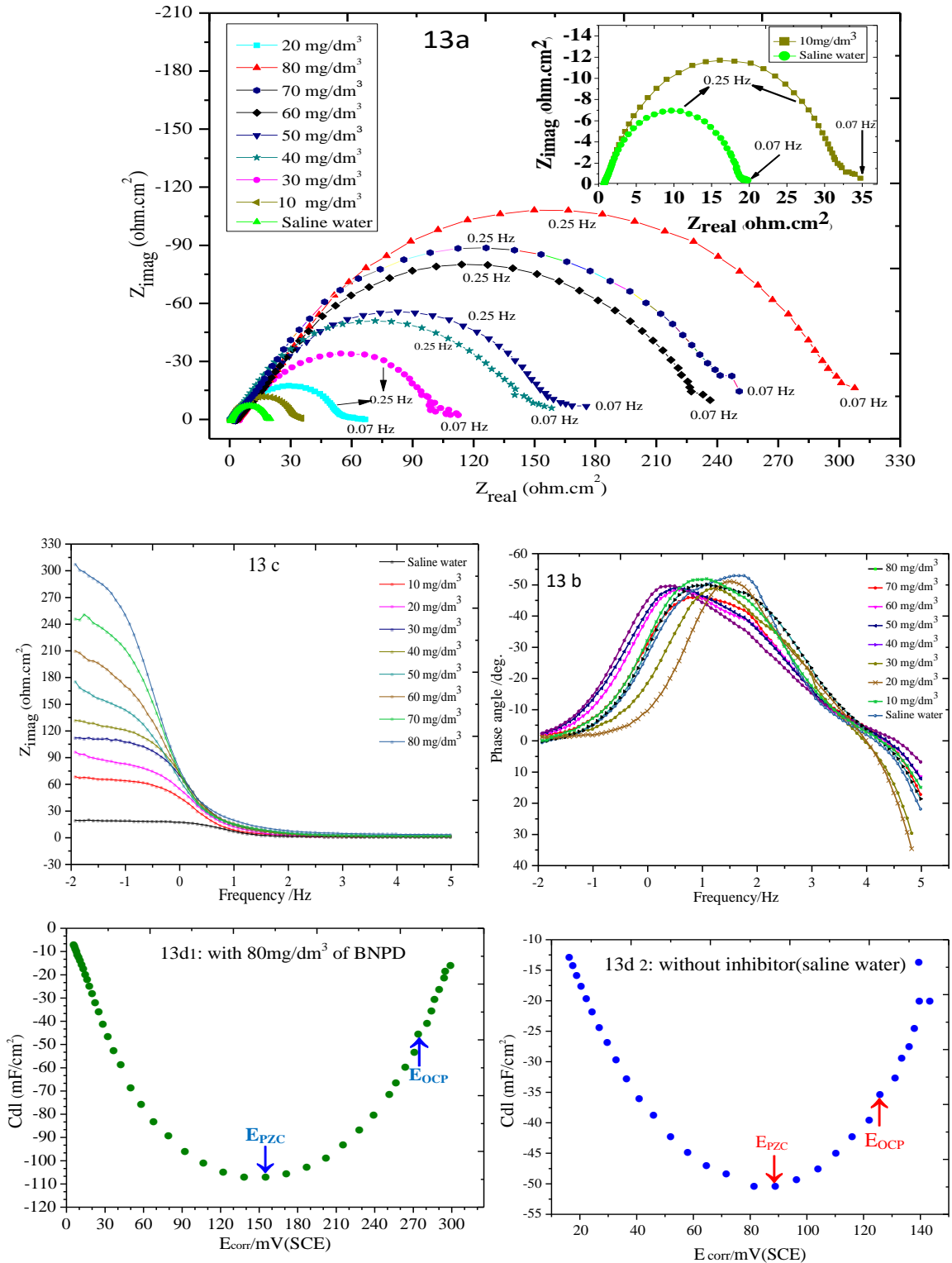
Fig.13: Typical EIS spectra, (a)Nyquist diagrams, (b)Bode-phase angle plots, (c)AC impedance Bode plots, (d) plots of capacitance vs. applied electrode potential for carbon steel corrosion in saline water.

**Table 1.** EIS data of carbon steel corrosion in the absence and presence of BNPD inhibitor at 308K (±1).

Inhibitor Con. (mg.dm^{-3})	f_{max} (Hz)	C_{dl} (μF/cm^2)	R_{ct} (Ω cm^2)	R_s (Ω cm^2)	R'_{ct} (Ω cm^2)	E_I (%)	θ	τ_d (s)	C_R (mpy)	E_{ocp} (mV/SCE)	PZC (mV/SCE)	E_P (mV)
Saline water	55.22	145.34	19.84	0.77	19.07	---	---	0.00288	2.188	125.71	88.81	+36.9
10	43.07	106.36	34.76	0.79	33.97	43.0	0.430	0.00369	1.129	---	---	---
20	33.18	71.95	66.70	0.65	66.05	70.3	0.703	0.00479	1.014	---	---	---
30	28.34	49.93	112.52	0.81	111.71	82.4	0.824	0.00561	0.845	---	---	---
40	24.76	40.59	158.42	0.46	157.96	87.5	0.875	0.00643	0.632	---	---	---
50	23.77	38.17	175.50	0.63	174.87	88.7	0.887	0.00669	0.564	---	---	---
60	19.99	33.69	236.41	0.55	235.86	91.7	0.917	0.00796	0.446	---	---	---
70	18.98	33.43	250.92	0.71	250.21	92.1	0.921	0.00838	0.283	---	---	---
80	17.11	30.25	307.62	0.88	306.74	93.6	0.936	0.00930	0.193	273.78	155.11	+118.67

3. 3. Results of inhibition by weight loss method

The BNPD molecules were evaluated as corrosion inhibitors in oil fields using the weight loss method. Weight loss and corrosion rate of the carbon steel have been calculated after its immersion in saline water for 3 hours at 308K (±1). Also, inhibition efficiency and the surface of covered carbon steel by inhibitor molecules have been calculated as listed in Table 2. The value of weight loss was calculated for two separate samples under the same conditions then the weight loss average was calculated for them. Weight loss in an inhibitor absence was noted that it was larger than in its presence. When the increase of NBPD concentration, the corrosion rate and weight loss decreased irregularly, due to the difference in corrosion outputs that accumulated on the surface of carbon steel. BNPD inhibitor shows excellent performance against corrosion where its maximum efficiency reached 91.14%. This is due to the physical adsorption of BNPD molecules on the carbon steel surface through the interaction between π- bonds of the aromatic system in NBPD and the effective positive centers of the metal surface. Or due to the chemical adsorption emergence through coordinated bond formation between free electron pairs of the nitrogen and sulfur atoms in BNPD and/or π-electrons of BNPD and the d-orbital of the iron atoms [17,49]. Fig.14 showed an increased curve of inhibition efficiency with a decreased curve of corrosion rate at the increased NBPD concentration.

Table 2. Results of weight loss experiments in the absence and presence of BNPD at 308K (±1)

Inhibitor Con. (mg.dm^{-3})	Weight loss (mg)	Corrosion rate (mg cm^{-2} h^{-1})	Surface coverage	Inhibition efficiency
Saline water	0.779	4.99×10^{-3}	----	----
10	0.402	2.57×10^{-3}	0.4849	48.49
20	0.361	2.31×10^{-3}	0.5370	53.70
30	0.301	1.93×10^{-3}	0.6132	61.32
40	0.225	1.44×10^{-3}	0.7114	71.14
50	0.201	1.28×10^{-3}	0.7434	74.34
60	0.159	1.01×10^{-3}	0.7975	79.75
70	0.101	6.47×10^{-4}	0.8703	87.03
80	0.069	4.42×10^{-4}	0.9114	91.14
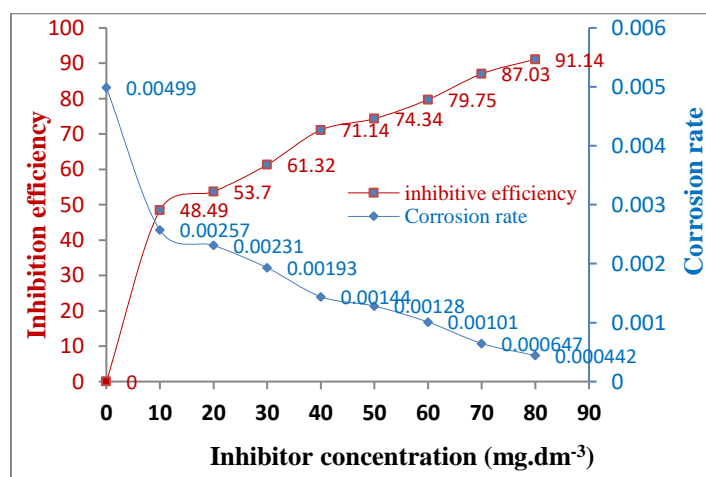
Fig.14. Effect of BNPD concentration on curves of corrosion rate and inhibition efficiency at 308K (±1)

3. 4. Results of potentiodynamic polarization methodology

The BNPD compound as a corrosion inhibitor has been evaluated by using the potentiodynamic polarization technique after immersing samples in the corrosive environment for 3 hrs. at 308K (±1). From Tafel curves, some electrochemical parameters have been calculated, like corrosion current density (I_{corr}), corrosion potential (E_{corr}), corrosion rate(C_R), potential displacement (ΔE_{corr}), anodic Tafel slope (βa), cathodic Tafel slope (βc) and inhibition efficiency (E_I). Also from linear polarization resistance (LPR), the polarization resistance (R_p) and inhibition efficiency ($\eta\%_{R_p}$) have been calculated as demonstrated in Table 3. The type of inhibitor depends on the potential displacement. If it is greater than 85 mV toward the anode compared with a blank can be considered an anodic-type inhibitor, whereas if it is greater than 85 mV toward the cathode can be regarded as a cathodic-type inhibitor. Otherwise, it is considered a mixed-type inhibitor [46,50]. The data of ΔE_{corr} clarifies that a maximum displacement of potential is 36 mV at 60 mg.dm^{-3} and it is far less than 85 mV. Hence, potential displacement indicates that the BNPD compound controls each of the anodic and cathodic reactions. Therefore, BNPD can be considered a mixed-type inhibitor as evident in Fig.15(c) and Table 3. Polarization curves show that the addition of an inhibitor led to a shift in the corrosion potential

toward the less negative region (slight negative shift). In other words, the Tafel curves have changed at the micro-scale for a small area within the potential, the change is from $-$ 0.292 V to $-$ 0.328 V as a maximum value as evident in Fig.15(a) and Table 3 [46,50-52]. Regarding the data in Table 3, the density of the corrosion current has decreased remarkably in the presence of the BNPD inhibitor, from 2.897 mA.cm^{-2} to 0.604 mA.cm^{-2} when its concentration increased from 10 mg.dm^{-3} to 70 mg.dm^{-3} respectively. While using 80 mg.dm^{-3} of inhibitor, the lowest value of I_{corr} (0.531 mA.cm^{-2}) was obtained. Such a value has given a maximum inhibition efficiency of 93.46%. Due to forming the passive layer on the carbon steel surface which is more stable [50,51,53]. Or owing to the formation of the coordinate bonds between unshared electrons of nitrogen, oxygen, sulfur and unoccupied *3d* orbitals of iron atoms. Simultaneously, the molecules of the inhibitor will accept the electrons from anti-bonding orbitals of the iron atoms to form the back-donation bonds [7,54]. The values of corrosion potential in the inhibitor presence are lower than in its absence, this implies that the inhibitor absence has made the corrosion process faster or starts early compared with inhibitor presence. From another aspect, the molecules of BNPD enhance the resistance to corrosion and delay the corrosion process [55]. The value of each of the anodic Tafel slope and cathodic Tafel slope has significantly decreased at inhibitor addition in comparison with its absence (saline water), which means the inhibitor has changed the corrosion mechanism [56]. This confirms that the inhibitor affects both anodic and cathodic reactions simultaneously through its adsorption on the effective sites uniformly. This is to say that BNPD is a mixed-type inhibitor [46,47]. The polarization resistance in the absence of an inhibitor is less than in its presence, as evident in Table 3 and the linear polarization curves in Fig.15(b). It can be observed that inhibition efficiency η%$_{Rp}$ has increased with increasing polarization resistance to reach 93.12% [39,47].
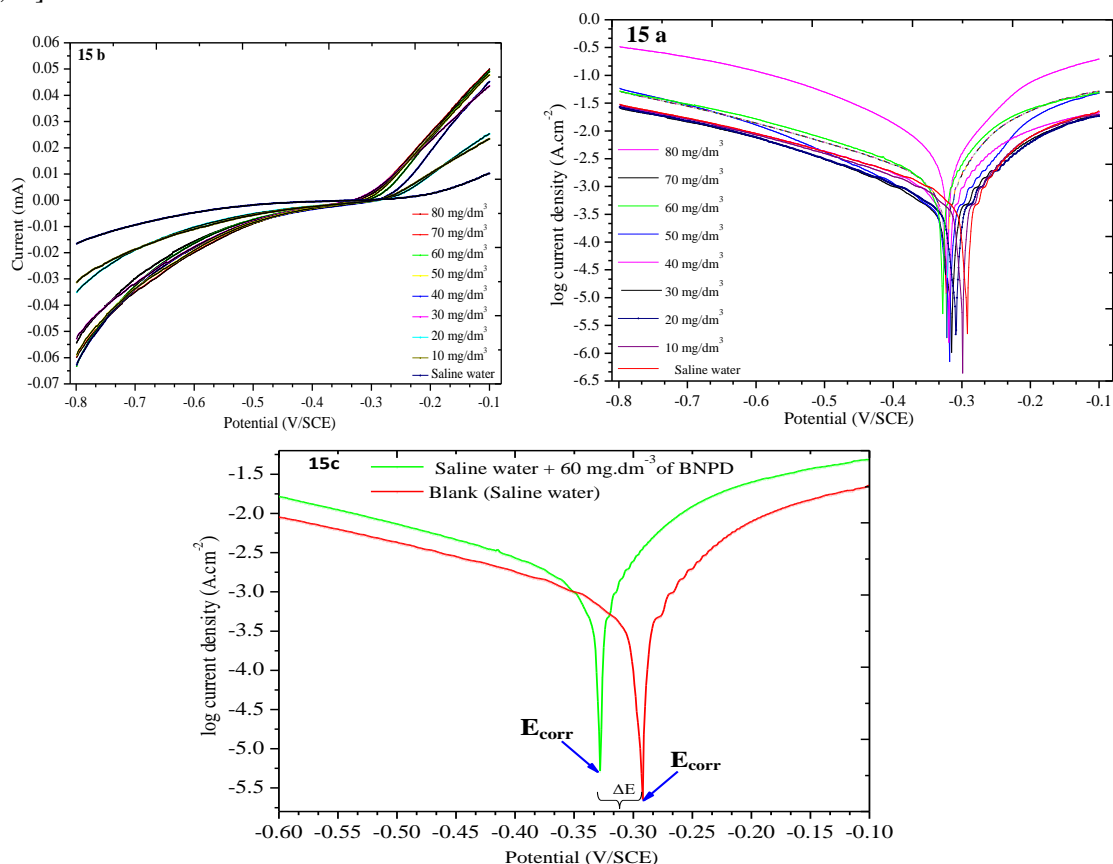

Fig.15. Typical polarization curves, (a)Tafel plots, (b) linear polarization curves, and (C) maximum shift of potential for carbon steel corrosion in saline water.

Table3. Polarization data of N-80 corrosion in the absence and presence of BNPD inhibitor at 308 K (±1)

Inhibitor Con. (mg.dm^{-3})	Polarization parameters								Linear polarization parameters	
	I_{corr} (mA .cm^{-2})	E_{corr} (mV/SCE)	βa (V.dec^{-1})	βc (V. dec^{-1})	C_R mpy) (	ΔE_{corr} (mv)	θ	E_I (%)	R_p (Ω cm^2)	η%$_{R_p}$
Saline water	8.131	-292	87.21	98.54	2.988	-----	-----	-----	68.56	----
10	2.897	-299	38.91	45.21	1.222	-7	0.6437	64.37	196.11	65.04
20	2.051	-309	32.01	41.98	1.211	-17	0.7477	74.77	266.02	74.22
30	1.921	-315	28.65	38.98	0.892	-23	0.7637	76.37	289.99	76.35
40	1.899	-319	25.61	32.64	0.755	-27	0.7664	76.64	295.93	76.83
50	1.405	-326	21.39	29.76	0.651	-34	0.8272	82.72	398.26	82.78
60	1.331	-328	19.03	26.23	0.564	-36	0.8363	83.63	410.44	83.29
70	0.604	-316	17.16	22.94	0.345	-24	0.9257	92.57	888.99	92.28
80	0.531	-322	14.62	19.01	0.261	-30	0.9346	93.46	997.13	93.12

3.5. Analysis results of SEM and EDX.

To establish (i) the morphology of metallic surface and distortions caused by corrosion, (ii) the percentage of elements in metal, and (iii) inhibitor effectiveness the SEM/EDX technique has been studied. To confirm the electrochemical results, the SEM/EDX experiments were carried out at an optimum concentration of inhibition after samples immersion in saline water for 3 hrs in the presence of 80 mg.dm^{-3} of inhibitor. Fig.16(a) showed the surface of polished carbon steel, was that the surface smooth was noticed and did not contain distortions. Also, Fig.16(a) showed the element's proportions of the N-80 and their distribution before immersion in saline water (reference), where the elementals distribution showed peaks for iron, carbon, and oxygen, in addition to peaks for other elements, indicating a high proportion of the iron, reached to 98.36%. The microscopic image and x-ray spectrum for the surface of carbon steel after its immersion in saline waters without inhibitor were shown in Fig.16(b), where uniform corrosion considerably was noted on the N-80 surface, like the distortions, roughness, cracks, significant pits, etc. This means the N-80 surface was damaged due to the effect of the aggressive ions, present in saline water at high concentrations like chloride ion 164599 mg/l and sulfate ion 1987 mg/l, where corrosion is considered more serious. Meanwhile, the EDX spectrum showed peaks for iron, carbon, oxygen, and peaks for other elements. The percentage of iron (iron amount) decreased was noted considerably with the percentage increased each of carbon and oxygen as corrosion products. This confirms the carbon steel corrosion without inhibitor where its surface is unprotected. Fig.16(c) showed the carbon steel surface and its spectrum after its immersion in saline waters contented on 80 mg.dm^{-3} of BNPD inhibitor where slight corrosion appeared and less severe distortions. Due to the layer formation of BNPD molecules and their adsorption on the carbon steel

surface. Where the surface became more homogeneous and smoother compared to the unprotected surface 16(b) but is similar to a large extent to the polished surface 16(a). The spectrum of the EDX with inhibitor presence showed a few decreases in the content of Fe 16(c) due to the effectiveness of the BNPD molecules where corrosion became imperceptible. The EDX spectrum of the polished surface is similar approximately to the spectrum of the protected surface due to the splendid inhibition. The percentage of each of the iron, oxygen, and carbon in polished N-80 (reference) is 98.36%, 2.11%, and 3.72%, respectively. After the N-80 was immersed in the corrosive environment without an inhibitor, the proportion of iron decreased to 89.31%, while the proportion of each carbon and oxygen increased to 16.52% and 22.53%, respectively caused by the corrosion of N-80. Corrosion processes decreased at the inhibitor addition, where a proportion each of iron, oxygen, and carbon slightly changed as follows 97.55%, 9.12%, and 6.42%, and they are near from proportions of the N-80 polished as evident in Table 4. Therefore, the percentage of corroded iron has decreased by 8.38% due to inhibitor effectiveness where the percentage of inhibition efficiency reached 91.08% [57-62].

Table 4. The percentage of important elements in N-80 at 308 K ($\pm$1)

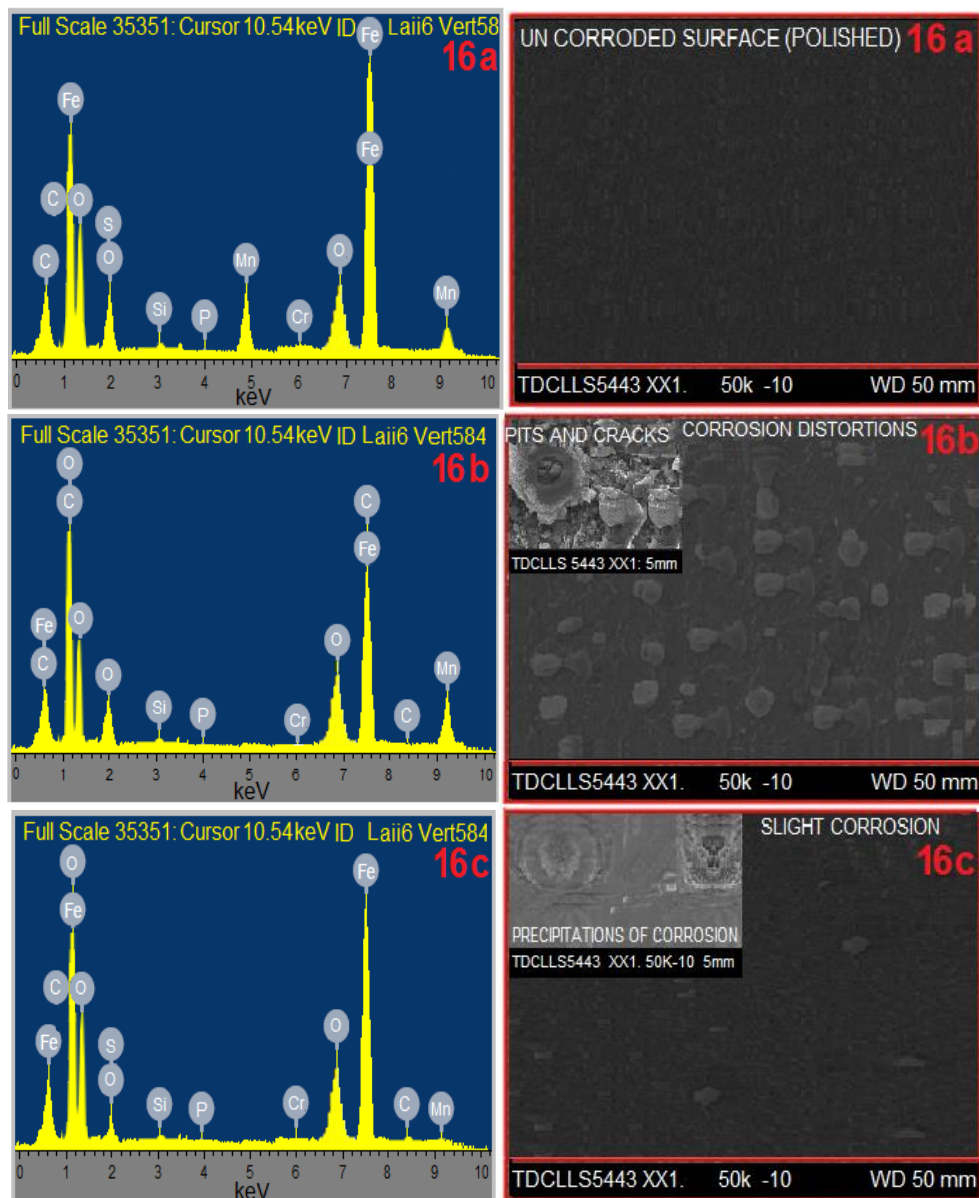| Carbon steel (N-80)	Reference (Fresh)	Without inhibitor	With 80 mg.cm^{-3} of inhibitor
Iron element (%)	98.36	89.31	97.55
Oxygen element (%)	2.11	22.53	9.12
Carbon element (%)	3.72	16.52	6.42
Percentage of corroded iron	-------	9.20	0.82
Inhibitor efficiency (%)	-------	------	91.08

Fig.16. The microscopic images and spectra of elements analysis for carbon steel at (a) polished, (b) without inhibitor, (c) with inhibitor at 308 K ±1.

3.6 Physic-chemical and electronic characteristics of BNPD inhibitor.

After evaluation of the compound 5-benzyl-5-((5-nitropyridin-3-yl) methyl)-1,3,5-dithiazinan-5-ium as an excellent inhibitor for resisting carbon steel corrosion. It is necessary to know its characteristics electronic and physic-chemical analyzed in the Gaussian 03W software using the DFT/B3LYP method with 6-31G (d,p) basis sets. The calculated characteristics are dipole moment (μ) 2.44 Debye; solvation energy(SE) 79.34 kJ/mol; Lipophilicity coefficient 0.32; molecule surface area 482.41Å^2; molecular volume 788.12Å^3; molar refractivity 89.77; molecular polarizability 23.45 Å^3; highest occupied molecular orbital (HOMO) where $E_{HOMO}= -7.865eV$; lowest unoccupied molecular orbital (LUMO) where $E_{LUMO}=-0.821eV$; energy gap (ΔE_{gap}) where $\Delta E_{gap}= 7.044eV$; total energy – 1030.23 eV; and electrostatic potential surface (EPS). The EPS of the BNPD molecules has been displayed in different colors in the electrostatic map within a range from dark red to dark blue. The color red represents the rich region in electrons (nucleophilic), whereas the color blue on the contrary,

where the poor region in electrons represents (electrophilic) as evident in Fig.17. Also, this figure showed the optimized structure, the electronic distribution density of HOMO and LUMO for BNPD inhibitor. Furthermore, the theoretical inhibition efficiency has been calculated depending on the relation $IE_{Theor} = 123.418 - (9.334 \times \mu) - (0.131 \times SE)$[63], which reached 90.25% and it is identically almost to the experimental inhibition efficiency.
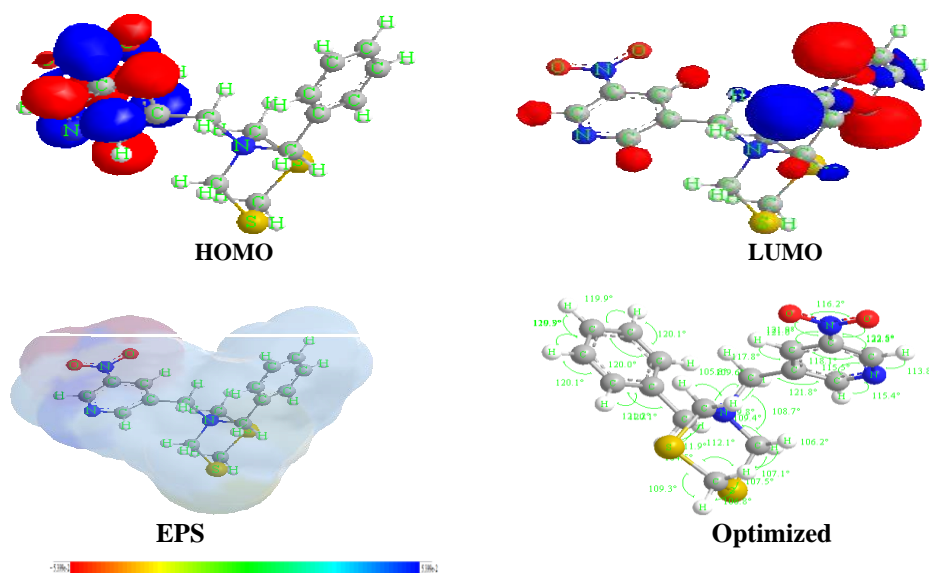

Fig.17. Electrostatic potential surface EPS at isopotential value ±5.399e-2 a.u., optimized geometry structure, HOMO and LUMO of the BNPD compound.

4. Conclusions and future recommendations

This study reveals the excellent performance of the compound 5-benzyl-5-((5-nitropyridin-3-yl) methyl)-1,3,5-dithiazinan-5-ium as an inhibitor for the corrosion of carbon steel. The maximum efficiency of the compound has reached 93.6 %. The experimental results of each technique of EIS, PP, SEM/EDX, and WL agree with each other. Results of polarization refer that the BNPD acts as a mixed-type inhibitor and the BNPD affects each anodic dissolution and cathodic evolution. The inhibition efficiency of BNPD increases with its concentration increase. The SEM/EDX technique confirms the adsorption of BNPD molecules on the surface of carbon steel and protects the surface from corrosion. The compounds that possess in their structures hetero atoms have high inhibition characteristics in saline water. The EIS results demonstrate that the BNPD inhibitor has the possibility of configuring a protective film on the N-80 surface. According to the results of PZC and E_{ocp}, we conclude that the excess potential on the surface is positive. The molecules, which have low energy in molecular orbitals of HOMO and LUMO, possess excellent inhibition properties. Carbon steel has been inhibition by physical and chemical adsorption simultaneously. The experimental inhibition efficiency and its theoretical efficiency are identical.

In conclusion, we recommend the following: (i) applying BNPD inhibitor practically in oil fields, (ii) applying BNPD inhibitor in the laboratory on various minerals in different corrosive environments with high flow, high temperatures, and high pressure, (iii) preparing similar inhibitors to the current inhibitor.

5. References

[1]   R.P. Bothi, R.A. Abdul, O. Hannah, A. Khalijah, Acta Phys.-Chim. Sin. **26**(8), 2171 (2010). Doi:https://doi.org/10.3866/PKU.WHXB20100646.

[2]   R.G. Sundaram, M. Sundaravadivelu, Int. J. Chem Tech Research **9**(3), 527 (2016).

[3]   L.T. Popoola, A.S. Grema, G.K. Latinwo, B. Gutti, A.S. Balogun, Int. J. Ind. Chem. **4**(35),1 (2013). Doi:https://doi.org/10.1186/2228-5547-4-35

[4]   R.W. Revie, H.H. Uhlig. (2008). Corrosion and corrosion control, 4th edition, John Wiley and Sons, Canada.

[5]   M. Ayazi, S. Mirfenderski, A.A. Moghadam, M.R. Monavarian, Petroleum and Coal **48**(2),6 (2006).

[6]   X. Jiang, Y.G. Zheng, D.R. Qu, W. Ke, Corros. Sci. **48**(10), 3091 (2006). Doi:https://doi.org/10.1016/j.corsci.2005.12.002

[7]   S.A. Ali, M.A.J. Mazumder, M.K. Nazal, H.A. Al-Muallem, Arabian J. Chem. **13**, 242 (2020). Doi:https://doi.org/10.1002/pola.21624

[8]   S. papavinasam. (2000). Corrosion inhibitors, 2rd edition, John Wiley and Sons, Inc., Ottawa, Ontario, Canada.

[9]   H. Serrar, M. Larouj, H.L. Gaz, Z. Benzekri, A. Zarguil, H. Essebaai, S. Boukhris, H. Oudda, R. Salghi, A. Hassikou, A. Souizi, Portugaliae Electrochimica Acta **36**(1),35 (2018).

[10] S. Chitra, K. Parameswari, A. Selvaraj, Int. J. Electrochem. Sci. **5**, 1675 (2010).

[11] M.J. Meften, Thi-Qar J. of Science **7**(1), 103 (2019).

[12] K. Alaoui, Y. El Kacimi, M. Galai, H. Serrar, R. Touir, S. Kaya, C. Kaya, M. Ebn Touhami, Int. J. Industrial Chem. **11**, 23 (2020). Doi:https://doi.org/10.1007/s40090-019-00199-5

[13] H. Lgaz, R. Salghi, I.H. Ali, Int. J. Electrochem. Sci. **13**, 250 (2018). Doi:https://doi.org/10.20964/2018.01.26

[14] G. Gece, Drugs, Corros. Sci. **53**, 3873 (2011). Doi:https://doi.org/10.1016/j.corsci.2011.08.006

[15] M.B. Harb, S. Abubshait, N. Etteyeb, M. Kamoun, A. Dhouib, Arabian J. Chem. **13**, 4846(2020). Doi:https://doi.org/10.1016/j.arabjc.2020.01.016

[16] B.M Mistry, N.S Patel, S. Jauhari **3**(5),300(2011).

[17] M. J. Meften, "synthesis of some new heterocyclic compounds through domino reaction, identification, and study of them as corrosion inhibitors for carbon steel alloy in acidic medium, and brine water," Ph.D. thesis, Department of chemistry, University of Basrah, Basrah, Iraq (2014).

[18] B. Nammalwar, R.A. Bunce, molecules **19**, 204 (2014). Doi:https://doi.org/10.1039/P19800002105

[19] L.F. Tietze. (2013). Domino reactions, 6th edition, Wiley-VCH Verlag GmbH and Co. KGaA, Germany. Doi:https://doi.org/10.1002/9783527671304

[20] M.J. Meften, A.S. Abdulnabi, Int. J. Eng. Tech. Res. **2**(12),7 (2014).

[21] T.J.J. Müller, D.M. Souza, Pure Appl. Chem. **8**(3),609 (2008).

[22] M. Yadav, D. Behera, U. Sharma, Arabian J. Chem**. 9**, 1487 (2016). Doi:http://doi.org/10.1016/j.arabjc.2012.03.011

[23] S.K. Ahmed, W.B. Ali, A. A. Khadom, Int. J. Ind. Chem. **10**, 159 (2019). Doi:https://doi.org/10.1007/s40090-019-018-8

[24] P.R. Ammal, M. Prajila, A. Joseph, Egyptian J. Petroleum **27,**307 (2018). Doi:https://doi.org/10.1016/j.ejpe.2017.05.002

[25] N. Wazzan, I.B. Obot, H. Faidallah, Int. J. Electrochem. Sci. **14**, 7450 (2019). Doi:https://doi.org/10.0964/2019.08.02

[26] X. Wang, J. Xing, Int. J. Electrochem. Sci. **15**, 1606 (2020). Doi:https://doi.org/10.20964/2020.02.46

[27] A.S. Fouda, H.M. Elabbasy, Int. J. Electrochem. Sci. **14**, 6884 (2019). Doi:https://doi.org/10.20964/2019.07.31

[28] O.S. Yadav, S. Kumar, G. kaur, G. Singh, Heterocyclic Letters **4**(2),251 (2014).

[29] S. John, A. Joseph, Materials Chem. Physics. **133**, 1083(2012). Doi:https://doi.org/10.1016/j.matchemphys.2012.02.020

[30] H.M. Elabbasy, Int. J. Electrochem. Sci. **14**, 5355(2019). Doi:https://doi.org/10.20964/2019.06.23

[31] G.G. Sánchez, N.V. Likhanova, P. Lozada, J. A. Morales, N. Nava, O.O. Xometl, I.V. Lijanova, G. Corro, Int. J. Electrochem. Sci. **14**, 9255 (2019). Doi:https://doi.org/10.20964/2019.09.65

[32]   K.C. Emregül, O. Atakol, Materials Chem. Phys. **83**, 373 (2004). Doi:https://doi.org/10.1016/j.matchemphys.2003.11.008

[33]   B. Stuart. (2004). Infrared spectroscopy: Fundamentals and applications, John Wiley & Sons.

[34] D.L. Pavia, G.M. Lampman, G.S. Kriz. (2001). Introduction to spectroscopy, 3th edition, Thomson Learning Inc, USA.

[35] E. Pretsch, P. Buhlmann, M. Badertscher. (2009). Structure determination of organic compounds, 4th edition, Springer-Verlag Berlin Heidelberg. Doi:https://doi.org/10.1007/978-3-540-93810-1

[36] A.S. Fouda, M. Abdel Azee, S.A. Mohamed, A. El-Hossiany, E. El-Desouky, Int. J. Electrochem. Sci. **14**, 3932 (2019). Doi:https://doi.org/10.20964/2019.04.44

[37]   S. Chen, B. Zhu, X. Liang, Int. J. Electrochem. Sci. **15**,1(2020). Doi:https://doi.org/10.20964/2020.01.39

[38]   S. Chen, S. Chen, W. Li, Int. J. Electrochem.Sci. **14**, 11419 (2019). Doi:https://doi.org/10.20964/2019.12.36

[39]   A.K. Singh, M.A. Quraishi, Int. J. Electrochem.Sci. **7**,3222 (2012).

[40]   J. Hu, D. Zeng, Z. Zhang, T. Shi, G. Song, X. Guo, Corros. Sci. **74**,35 (2013). Doi:https://doi.org/10.1016/j.corsci.2013.04.005

[41]   K. Zhang, L. Wang, G. Liu, Corros. Sci. **75**,38(2013). Doi:https://doi.org/10.1016/j.corsci.2013.05.014

[42]   J. Wang, L. Zhang, Y. Gao, X. Liu, W. Hu, Int. J. Electrochem. Sci. **14**,59 (2019). Doi:https://doi.org/10.20964/2019.01.24

[43]   S. Wang, J. Yang, J. Cao, L. Gao, C. Yan, Int. J. Electrochem.Sci. **14**, 9671 (2019). Doi:https://doi.org/10.20964/2019.07.17

[44]   M.J. Meften, Int. J. of Innov. Res. Sci. Eng. Tech. **5**(7), 13685 (2016). Doi:https://doi.org/10.15680/IJIRSET.2016.0507227

[45] H. Elmsellem, K. Karrouchi, A. Aouniti, B. Hammouti, S. Radi, J. Taoufik, M. Ansar, M. Dahmani, H. Steli, B. El Mahi, Der Pharma Chemica **7**(10), 237 (2015).

[46] N.B. Iroha, L.A. Nnanna, J. Mater. Environ. Sci. **10**(10), 898 (2019).

[47]   K.S. Shaju, K.J. Thomas, V.P. Raphael, A. Paul **(ID 820548)**,1 (2013). Doi:https://doi.org/10.1155 /2013/820548

[48]   H. Liu, Y. Dai, Y.F. Cheng, Arab. J. Chem. **13**, 3601 (2020). Doi:https://doi.org/10.1016/j.arabjc.2019.11.006

[49]   Y. Yang, H. Liu, D. Lu, L. Peng, L. Wang, Int. J. Electrochem. Sci. **14**, 5008 (2019). Doi:https://doi.org/10.20964/2019.06.17

[50]   L. Adardour, H. Lgaz, R. Salghi, M. Larouj, S. Jodeh, M. Zougagh, O. Hamed, M. Taleb, Der Pharmacia Lettre **8**(4), 173 (2016).

[51] A. Fateh, M. Aliofkhazraei, A.R. Rezvanian, Arab. J. Chemis. **13**, 481 (2020). Doi:https://doi.org/10.1016/j.arabjc.2017.05.021

[52]   S. Tokuda, I. Muto, Y. Sugawara, N. Hara, Corros.Sci. **167**,1(2020). Doi:https://doi.org/10.1016/j.corsci.2020.108506

[53]   V.A. Arizmendi-Salgado, S.A. Serna, A. Torres-Islas, R. Soto-Espitia, P. Althuzer, S. Mejia-Sintillo, J. Campos-Alvarez, J.G. Gonzalez-Rodriguez, Int. J. Electrochem. Sci. **14**, 8243 (2019). Doi:https://doi.org/10.20964/2019.08.102

[54]   M.J. Meften, Eur. J. Chem**.** **8**(3), 229 (2017). Doi:https://doi.org/10.5155/eurjchem.8.3.229239.1589

[55]   S.C. Soh, M. Aziz, R. Sundari, Ind. J. Sci. Res. and Tech. **2**(2), 25 (2014).

[56]   Y. Yang, Y. Li, L. Wang, H. Liu, D. Lu, L. Peng, Int. J. Electrochem. Sci. **14**, 3375 (2019). Doi:https://doi.org/10.20964/2019.04.18

[57] Q. Li, L. Dong, Y. Yang, Z. Wu, H. Zhu, Y. Dong, Y. Shen, L. Zhang, Q. Lu, Int. J. Electrochem. Sci. **15**, 470 (2020). Doi:https://doi.org/10.20964/2020.01.60

[58] M. J. Meften, N.Z. Rajab, M.T. Finjan, American Scien. Res. J. Eng. Tech. and Sci. **27**(1),419(2017).

[59]   S. Chitra, K. Parameswari, A. Selvaraj, Int. J. Electrochem. Sci. **5**, 1675 (2010).

[60] A.E. Vázquez, M.A.C. Robles, G.E.N. Silva, F.J.R. Gómez, M.P. Pardavé, L.L. Romero, D. A. Beltrán, D.P. Martínez, Int. J. Electrochem. Sci. **14**, 9206 (2019). Doi:https://doi.org/10.20964/2019.09.57

[61] D. Li, Z. Shi, H. Xu, Y. Chen, W. Feng, Z. Qiu, H. Liu, G. Lv, S. Wang, Y. Fan, Int. J. Electrochem. Sci. **14,** 3465 (2019). Doi:https://doi.org/10.20964/2019.04.47

[62] M.J. Meften, "Study of effect the seeds aqueous extracts of brassica niger and anthemis nobilis as corrosion inhibitors for carbon steel in acidic media," M.Sc. thesis, Department of chemistry, University of Basrah, Basrah, Iraq, 2011.

[63] M.J. Meften, W.A. Radhi, A.N. Abulhail, Basrah J. of Sci**. 36**(1),1 (2018). Doi:https://doi.org/10.29072/ basjs.2018302

تحضير 5- بنزيل -5 - ((5- نيتروبيريدين-3- يل) ميثيل) -5،3،1-دايثايازينان -5 -آيوم بواسطة تفاعلات الوعاء الواحد، تشخيصه ودراسته كمثبط للتآكل في حقول النفط عالية الملوحة

مشتاق جري مفتن، عمار عبد الجبار كاظم

قسم الكيمياء، كلية التربية ـــ القرنة، جامعة البصرة، البصرة، العراق.

معلومات البحث	الملخص

الملخص

تضمنت هذه الدراسة تحضير مركب حلقي غير متجانس جديد بطريقة فعالة بسيطة ومقبولة بيئيا وهي تفاعلات الدومينو. يحتوي المركب المحضر على ذرات غير متجانسة هي الاوكسجين والنتروجين والكبريت حيث تم إدخالها في التركيب الكيميائي بخطوة واحدة متكونه من عدة تحولات. تم تشخيص المركب المحضر باستخدام عدة تقنيات مثل مطيافية الاشعة تحت الحمراء ومطيافية الرنين النووي المغناطيسي وطيف كروماتوغرافيا الغاز وطيف الكتلة. تمت دراسة الجزيء المحضر كمثبط لتآكل الفولاذ الكربوني (N-80) والذي يستخدم بشكل عام في حقول النفط. درست فعالية المركب كمادة مانعة للتآكل في المياه المالحة التي تصاحب استخراج النفط الخام حيث احتوت تلك المياه على مواد صلبة مذابة تقدر بـ 239581 ملي غرام / لتر، ودالة الحامضية 6.1. تم تقييم المثبط بواسطة تقنية التحليل الطيفي للمقاومة الكهروكيميائية، وتقنية الاستقطاب الديناميكي الفعال، ومطيافية الاشعة السينية (SEM/EDX) وطريقة فقدان الوزن عند درجة حرارةK308. حيث اشارت النتائج ان كفاءة التثبيط تزداد مع زيادة تركيز المثبط. كما أظهرت نتائج الاستقطاب الديناميكي الفعال أن جزيئات المثبط المدروسة تعمل كمثبط من النوع المختلط، بينما أظهرت نتائج فقدان الوزن أن هذه الجزيئات تمتز على سطح الفولاذ الكربوني من خلال الامتزاز الفيزيائي والكيميائي في وقت واحد. علاوة على ذلك، تم حساب الخصائص الإلكترونية والفيزيائية والكيميائية لـ للمركب المحضر وهي EHOMO و ELUMOوفجوة الطاقة والطاقة الكلية ومساحة سطح الجزيء والحجم الجزيئي وقابلية الاستقطاب الجزيئي والانكسارية المولية وعزم ثنائي القطب وطاقة الذوبان وكفاءة التثبيط النظري. أظهر المركب BNPD نتائج رائعة في تثبيط التآكل، حيث بلغت كفاءته المثلى 91.14٪ و93.60٪ و93.46٪ لتقنيات WL وEIS و PP على التوالي اما الكفاءة النظرية وصلت الى 90.25 وهذا يعتبر تطابق عالي الدقة

*Corresponding author email : ammar.kadhim@uobasrah.edu.iq